HHS Public Access

Author manuscript

Nat Microbiol. Author manuscript; available in PMC 2019 August 01.

Published in final edited form as:

Nat Microbiol. 2019 February ; 4(2): 316–327. doi:10.1038/s41564-018-0298-0.

Fungal ligands released by innate immune effectors promote inflammasome activation during *Aspergillus fumigatus* infection

Benoit Briard[1], **Rajendra Karki**[1], **R.K. Subbarao Malireddi**[1], **Anannya Bhattacharya**[1], **David E. Place**[1], **Jayadev Mavuluri**[1], **Jennifer L. Peters**[2], **Peter Vogel**[3], **Masahiro Yamamoto**[4], and **Thirumala-Devi Kanneganti**[1,*]

[1]Department of Immunology, St. Jude Children's Research Hospital, Memphis, Tennessee 38105, USA.

[2]Cellular Imaging Shared Resource, St. Jude Children's Research Hospital, Memphis, Tennessee 38105, USA.

[3]Animal Resources Center and the Veterinary Pathology Core, St. Jude Children's Research Hospital, Memphis, TN, 38105, USA.

[4]Department of Immunoparasitology, Research Institute for Microbial Diseases, Laboratory of Immunoparasitology, World Premier International Immunology Frontier Research Center, Osaka University, 3-1 Yamadaoka, Suita, Osaka 565-0871, Japan.

Abstract

Invasive pulmonary aspergillosis causes significant mortality in immunocompromised individuals. Recognition of *Aspergillus fumigatus* by the host immune system leads to activation of the inflammasome, which provides protection against infection. However, the regulation of inflammasome activation at the molecular level is poorly understood. Here, we describe two distinct pathways that coordinatedly control inflammasome activation during *A. fumigatus* infection. The C-type lectin receptor (CLR) pathway activates both MAPK and NF-κB signaling, which leads to induction of downstream mediators such as the transcription factor IRF1 and also primes the inflammasomes. Toll-like receptor (TLR) signaling through adaptor molecules MyD88 and TRIF in turn mediates efficient activation of IRF1, which induces IRGB10 expression. IRGB10 targets the fungal cell wall, and the antifungal activity of IRGB10 causes hyphae damage, modifies the *A. fumigatus* surface and inhibits fungal growth. We also demonstrate that one of the major fungal PAMPs, β-glucan, directly triggers inflammasome assembly. Thus, the concerted activation of both TLRs and CLRs is required for IRF1-mediated IRGB10 regulation, which is a key event governing ligand release and inflammasome activation upon *A. fumigatus* infection.

[*]**Correspondence should be addressed to:** Thirumala-Devi Kanneganti, Department of Immunology, St. Jude Children's Research Hospital, MS #351, 262 Danny Thomas Place, Suite E7004, Memphis TN 38105-2794, Tel: (901) 595-3634;, Fax. (901) 595-5766. Thirumala-Devi.Kanneganti@StJude.org.

Author contributions

B.B., R.K., R.K.S.M., J.M., A.B., D.E.P., and J.L.P. performed the experiments; B.B., R.K., R.K.S.M., P.V., M.Y., and T.-D.K. analyzed the data. B.B., A.B., and R.K. wrote the paper. T.-D.K. oversaw the project and funding.

COMPETING INTERESTS

The authors declare no competing financial interests.

Data Availability

The data that support the findings of this study are available from the corresponding author upon request.

Keywords

Inflammasome; NLRP3; AIM2; caspase-1; Dectin-1; CLRs; *Aspergillus fumigatus*; fungi; IRF1; MyD88; TRIF; immunity-related GTPases; IRGB10; guanylate-biding proteins (GBPs); cell-autonomous immunity; innate immunity.

Invasive aspergillosis, a major cause of mortality in immunocompromised individuals[1-3], is caused by *Aspergillus fumigatus* (*A.f*). Innate immune system provides the first line of defense against inhaled *A.f* conidia. *A.f* is sensed by innate immune receptors such as membrane-bound Toll-like receptors (TLRs) TLR2, TLR3, TLR4 and TLR9 and C-type lectin receptors (CLRs) Dectin-1, Dectin-2, and DC-SIGN[4-11]. Cytosolic sensors such as Nod-like receptors (NLRs) and absent in melanoma 2 (AIM2)–like receptors (ALRs) are also involved in fungal sensing and host protection[12-22]. NLRP3 and AIM2 assemble the inflammasome, a multimeric protein complex mediating the cleavage of caspase-1, IL-1β and IL-18 and the induction of pyroptosis[23]. We previously showed that concerted activation of NLRP3 and AIM2 inflammasomes is required for effective caspase-1 activation and host resistance against *A.f* infection[17]. However, the regulation and activation of inflammasomes during *A.f* infection at the molecular level remain poorly understood.

Recent studies show multiple regulators of NLRP3 and AIM2 inflammasomes during cytosolic bacterial infections, such as the transcription factor IRF1 and downstream effector molecules of the interferon (IFN)–inducible GTPase family[24]. The GTPases guanylate-binding proteins (GBPs) and immunity-related GTPase B10 (IRGB10) target and lyse bacteria and liberate bacterial ligands, which ultimately triggers inflammasome activation[24-26]. Lipopolysacccharide (LPS) released by cytosolic bacteria leads to caspase 11–dependent activation of the non-canonical NLRP3 inflammasome[25,27], whereas DNA released upon bacterial lysis activates the AIM2 inflammasome[24-26]. Although the crucial role of IRF1 and IFN-inducible GTPases in inflammasome activation during bacterial infections is well established, the involvement of these proteins in inflammasome activation and host resistance during fungal infections remains to be investigated.

RESULTS

TLRs and Dectin-1 are required for inflammasome activation during *A.f* infection.

Host cells sense *A.f* via TLRs such as TLR2[8,28], TLR4[5,9,29], TLR3[4] and TLR9[6,10,30] and the CLR Dectin-1[31,32]. However, the role of TLRs and CLRs in inflammasome activation in response to *A.f* infection remains unknown.

We infected unprimed wild-type (WT), *Tlr2*$^{-/-}$, *Tlr3*$^{-/-}$, *Tlr4*$^{-/-}$, *Tlr9*$^{-/-}$ *Tlr2*$^{-/-}$ *Tlr4*$^{-/-}$ and *Tlr2*$^{-/-}$ *Tlr9*$^{-/-}$ bone marrow macrophages (BMDMs) with *A.f* and assessed caspase-1 activation and IL-1β release. Cleavage of caspase-1 and release of IL-1β were impaired in BMDMs lacking single TLR or multiple TLRs compared with WT BMDMs (Supplementary Fig. 1a,b,d,e), while the secretion of inflammasome-independent cytokine TNF was comparable among all genotypes (Supplementary Fig. 1c,f). These findings imply a key priming-independent role for TLRs in inflammasome activation upon *A.f infection.*

We also infected BMDMs lacking Dectin-1, a major CLR that binds to β1-3 glucans of *A.f* and is required for its clearance[33] with *A.f* and found decreased caspase-1 cleavage and IL-1β and TNF release, revealing a pivotal role for Dectin-1 in regulating both inflammasome priming and activation (Supplementary Fig. 1g-i). Overall, these results show both TLRs and Dectin-1 are required for inflammasome activation during *A.f* infection.

TRIF and Myd88 transduce signals for priming and activating the inflammasome during *A.f* infection.

The TLR adaptor proteins MyD88 and TRIF drive distinct signaling cascades necessary for immune responses against *A.f*[28,29,34]. We infected BMDMs lacking either MyD88, TRIF or both with *A.f.* and found reduction in Caspase-1 cleavage and IL-1β release in *Myd88*$^{-/-}$, *Trif*$^{-/-}$, and *Myd88*$^{-/-}$ *Trif*$^{-/-}$ BMDMs (Fig. 1a,b). However, TNF secretion was not impaired, suggesting that MyD88 and TRIF do not affect priming during *A.f* infection (Fig. 1c). Phosphorylation of both ERK1/2 and IκBα was also comparable between WT and *Myd88*$^{-/-}$ *Trif*$^{-/-}$ BMDMs (Fig. 1d). Consistent with this, WT and *Myd88*$^{-/-}$ *Trif*$^{-/-}$ BMDMs showed comparable induction of NLRP3 and IL1β after infection (Fig. 1e, Supplementary Fig. 2a), further confirming that MyD88 and TRIF are not required for inflammasome priming in cells infected with *A.f.*

The CLR, Dectin-1 transduces signals via the spleen tyrosine kinase (SYK), which in turn activates the CARD9–BCL10–MALT1 complex[33]. We adopted a genetic approach by using myeloid cells lacking SYK, hereby denoted as *Syk*$^{fl/fl}$*LysM*$_{Cre}$, as well as *Card9*$^{-/-}$ and *Malt1*$^{-/-}$ BMDMs. SYK deletion in BMDMs upon *A.f* infection was confirmed by western blotting (Fig. 1i). Similar to Dectin-1–deficient cells, there was reduced caspase-1 activation and IL-1β and TNF release in *Syk*$^{fl/fl}$*LysM*^{Cre}, *Card9*$^{-/-}$, and *Malt1*$^{-/-}$ BMDMs compared to WT BMDMs (Fig. 1f–h). The CLR pathway also regulates the activation of MAPK and canonical NF-κB signaling[33]. Indeed, the phosphorylation of ERK1/2 and I;κBα were substantially reduced in BMDMs lacking SYK, CARD9, MALT1 and Dectin-1 (Fig. 1i–k). In line with these findings, *Syk*$^{fl/fl}$*LysM*^{Cre}, *Card9*$^{-/-}$, and *Malt1*$^{-/-}$ BMDMs showed reduced induction of NLRP3 and IL1β after infection with *A.f* compared to WT cells (Supplementary Fig. 2b–f). These results demonstrate that SYK–CARD9–MALT1 pathway promotes inflammasome priming through MAPK and NF-κB signaling during *A.f* infection.

SYK–CARD9–MALT1 complex regulates IRF1 expression, whereas activation of IRF1 is MyD88/TRIF dependent.

IRF1 regulates inflammasome activation during cytosolic bacterial infections[24]. Activation of Dectin-1 and TLR2 promotes recruitment of IRF1 to the ISRE binding site to regulate gene expression[35]. BMDMs infected with *A.f* showed IRF1 induction (Fig. 2a) and induction of *Irf1* mRNA was reduced in *Syk*$^{fl/fl}$*LysM*^{Cre}, *Card9*$^{-/-}$, and *Malt1*$^{-/-}$ BMDMs compared with WT cells (Fig. 2a–c). *Irf1* expression was also reduced in *Dectin-1*$^{-/-}$ BMDMs compared to WT (Supplementary Fig. 3a). We also assessed whether the CLR pathway transcriptionally regulates IRF1 downstream genes *Irgb10* and *Gbp2* and we found significantly lower expression of *Gbp2* and *Irgb10* in BMDMs lacking CARD9 and MALT1 (Fig. 2d,e). The role of NF-κB signaling in *Irf1* expression has been previously reported[36]. Because the CLR pathway regulates NF-κB and MAPK signaling in response to *A.f* (Fig.

1i,j), we assessed IRF1 induction during fungal infection in the presence of the NF-κB inhibitor, Bay 11-7082. The phosphorylation of IκBα and IRF1 induction were reduced in BMDMs incubated with the NF-κB inhibitor (Fig. 2f). In contrast, both IRF1 mRNA and protein were similar between WT and *Myd88*$^{-/-}$ *Trif*$^{-/-}$ BMDMs infected with *A.f* (Fig. 2g,h), suggesting that TLR signaling is dispensable for IRF1 induction. Interestingly, despite similar *Irf1* expression, *Myd88*$^{-/-}$ *Trif*$^{-/-}$ BMDMs showed lower expression of *Gbp2, Gbp5* and *Irgb10* (Fig. 2i–k). The interaction between IRF1 and MyD88 is important for efficient nuclear localization of IRF1[35,37]. Indeed, we found reduction in IRF1 in the nuclear fraction of *A.f*-infected *Myd88*$^{-/-}$ and *Trif*$^{-/-}$ BMDMs compared to WT (Fig. 2l,m). Furthermore, overexpression of MyD88 increased IRF1 accumulation in the nuclear fraction compared to cells transfected with the vector control (Supplementary Fig. 3b–d). MyD88 and IRF1 co-precipitated during *A.f* infection in WT BMDMs whereas in cells lacking TRIF, the co-immunoprecipitation was reduced, although the expression of MyD88 was not affected (Supplementary Fig. 3e,f). These results demonstrated that SYK–CARD9–MALT1 complex regulates IRF1 expression downstream of NF-κB signaling, whereas MyD88 and TRIF signaling drives the nuclear translocation of IRF1.

IRF1 regulates inflammasome activation and the expression of GBPs and IRGB10 during *A.f* infection.

To investigate whether IRF1 is involved in regulating inflammasome activation during *A.f* infection, we infected *Irf1*$^{-/-}$ BMDMs with *A.f.* Processing of caspase-1 and release of IL-1β in *Irf1*$^{-/-}$ BMDMs were impaired after *A.f* infection (Fig. 3a,b). However, there was no significant difference in TNF secretion between *Irf1*$^{-/-}$ and WT BMDMs (Fig. 3c). The impaired inflammasome activation in *Irf1*$^{-/-}$ BMDMs could not be rescued after priming with LPS and β-glucan, confirming that inflammasome priming was not affected in the absence of IRF1 (Fig. 3d,e). IRF1 cooperates with IFN signaling and regulates the expression of IFN-inducible genes, particularly those encoding GBPs and IRGB10, which are important in mediating inflammasome activation during *F. novicida infection*[24,25]. We assessed the induction of GBP2, GBP5, and IRGB10 mRNA and protein in BMDMs after *A.f* infection. These GTPases were strongly induced in an IRF1-dependent manner (Fig. 3f–i), confirming the role of IRF1 in inducing GBPs and IRGB10 in response to *A.f* infection.

IRGB10, but not GBPs, contributes to the activation of inflammasomes in response to *A.f.*

The role of GBPs and IRGB10 in activating NLRP3 and AIM2 inflammasomes has been reported in multiple models of infection[38]. To investigate the role of GBPs and IRGB10 in *A.f* infection, we infected BMDMs lacking either IRGB10 or GBPs located on chromosome 3, namely GBP1, GBP2, GBP3, GBP5, and GBP7 (hereby denoted as *Gbp*$^{chr3-/-}$), with *A.f* and assessed inflammasome activation. BMDMs lacking IRGB10, but not GBPs, exhibited substantial reduction in caspase-1 activation and IL-1β release compared with WT cells infected with *A.f* (Fig. 4a–e). However, IRGB10 deficiency did not affect secretion of TNF (Fig. 4f). Consistently, phosphorylation of ERK1/2 and IκBα, and NLRP3 were similar between *Irgb10*$^{-/-}$ and WT BMDMs (Fig. 4g). The induction of *Il1b* and *Tnf* was also comparable between *Irgb10*$^{-/-}$ and WT BMDMs (Fig. 4h,i). Together these data demonstrate that the priming signal necessary for activation of inflammasome was not compromised in the absence of IRGB10. Moreover, caspase-1 cleavage was still impaired in

primed *Irgb10*$^{-/-}$ BMDMs compared to primed WT cells, further confirming a priming-independent role for IRGB10 (Fig. 4j and Supplementary Fig. 4a).

A.f engages both NLRP3 and AIM2 inflammasomes, and IRGB10 is known to be required for their activation during bacterial infection. To decipher whether the NLRP3 or AIM2 inflammasome contributes to the residual caspase-1 cleavage in *Irgb10*$^{-/-}$ BMDMs (Fig. 4d), we inhibited NLRP3 inflammasome with specific NLRP3 inhibitors, and caspase-1 cleavage was completely abolished in both conditions, suggesting that the NLRP3 inflammasome contributed to the residual caspase-1 cleavage in *Irgb10*$^{-/-}$ BMDMs (Supplementary Fig. 4b,c). The observed reduction in inflammasome activation could also be due to a defect in the phagocytosis and killing of conidia in *Irgb10*$^{-/-}$ BMDMs. WT and *Irgb10*$^{-/-}$ BMDMs showed comparable capability to phagocytose and kill resting conidia (Fig. 4k and Supplementary Fig. 4d). However, *Irgb10*$^{-/-}$ BMDMs demonstrated reduced capacity to inhibit hyphae growth (Fig. 4l). Together, these results suggest that IRGB10, independently of inflammasome priming and GBP function regulates the assembly and activation of inflammasomes during *A.f* infection.

IRGB10 directly targets intracellular *A.f.*

The IFN-inducible GTPases exert their antimicrobial actions by targeting cytosolic pathogens or microbes contained inside vacuoles38-40. We previously showed that GBPs and IRGB10 target the outer membrane of *E. coli* and *F. novicida* to release bacterial ligands and thereby facilitate inflammasome activation24,25. To investigate whether IRGB10 also targets *A.f*, we immunostained endogenous IRGB10 along with the fungal cell wall component chitin in BMDMs infected with the fungi. IRGB10 was induced upon *A.f* infection compared to unstimulated BMDMs (Supplementary Fig. 5a,b, Fig. 3f,i) and IRGB10 puncta accumulated around the cell wall of *A.f* (Supplementary Fig. 5b). The fluorescence projection revealed peak signals of IRGB10 immunostaining and the fungal cell wall staining superposed with each other (Supplementary Fig. 5c).

A.f is a pulmonary pathogen that can infect both immune and non-immune cells[17,41]. IRGB10 expression was upregulated in primary lung fibroblasts (LFs) upon infection with *A.f* in an IRF1-dependent manner (Supplementary Fig. 5d,e). Consistent with our observation in BMDMs, IRGB10 localized on the fungal cell wall in primary LFs infected with *A.f*, suggesting a role for IRGB10 in both immune and non-imune cells (Supplementary Fig. 5f,g) and distinct puncta of IRGB10 surrounding the *A.f* cell wall were observed (Fig. 5a–c). Similar to endogenous IRGB10, mCherry-tagged IRGB10 colocalized with *A.f* cell wall (Supplementary Fig. 5h,i). These observations indicate that the targeting of the fungal cell wall, which causes release of ligands, is the potential mechanism by which IRGB10 promotes inflammasome activation and host defense against *A.f.*

IRGB10 peptides inhibit *A.f* and liberate fungal ligands which induce inflammasome activation.

The role of IRGB10 in inflammasome activation has been reported, but its mode of action has not been explained25. Bioinformatic analysis of IRGB10 revealed two putative transmembrane helices with antimicrobial properties25. Further, we identified a new

antimicrobial strech between residues 170 and 186 with low probability of misclassification (Supplementary Fig. 6a,b). Indeed, this putative antimicrobial stretch is highly conserved among other members of the IRG family (Supplementary Fig. 6c). However, in comparison to all the other IRG family members for putative antifungal function, IRGB10 revealed the strongest antimicrobial; antifungal, antibacterial and antiviral activity (Supplementary Fig. 6d,e). Based on our analysis, we synthesized the putative antimicrobial peptides (Supplementary Fig. 6f, Supplementary Fig. 7a–f) and investigated their antifungal activities against *A.f.* The two putative transmembrane C-terminal peptides (1 and 2) showed antifungal activity against *A.f* whereas the scramble peptides 1 and 2 did not (Fig. 6d). Additionally peptide 3 that contains the putative antimicrobial stretch demonstrated antifungal activity and inhibited the growth of *A.f.* However a similar effect was also observed with the scrambled peptide 3 (Fig. 6e). This could be due to the structural properties of the scrambled peptide since the prediction method for the antimicrobial stretch was based on the amino-acid composition and not its sequence or three-dimensional structure. To further confirm the specific activity of these peptides, we selected 2 random IRGB10 peptides and tested their antifungal activity (Supplementary Fig. 6f and Supplementary Fig. 8a-d). These random peptides did not show any inhibitory activity against *A.f* (Fig. 6f). Although IRGB10 peptides induced hyphal damage, we did not observe any fungicidal activity on *A.f* resting conidia (Fig. 6g,h). This is in line with the activity observed previously in *Irgb10*$^{-/-}$ BMDMs (Fig. 4k,l). We further confirmed by scanning electron microscopy that the surfaces of hyphae were compromised by IRGB10 peptides compared to the control peptides (Fig. 5i). This led us to hypothesize that IRGB10 peptides induce the release of fungal PAMPs to activate the inflammasomes. Either the fungal polysaccharides or the DNA released into the cytoplasm by IRGB10 during intracellular *A.f* growth would lead to inflammasome activation. *A.f* DNA has been shown to engage the AIM2 inflammasome[17], however the role of fungal polysaccharides released into the cytoplasm in inducing inflammasome activation has not been explored. Transfection of β-glucan directly into the cytoplasm activated caspase-1 (Fig. 5j). However ,the capability to β-glucan to activate inflammasome still required IRGB10, indicating an IRGB10-dependent mechanism acting on β-glucan to facilitate inflammasome activation. Together, these data suggest that antimicrobial activity of IRGB10 disrupts fungal cell wall, leading to release of polysaccharides that facilitate inflammasome activation. The cell wall damage could possibly lead to lysis of fungal cell wall and subsequent release of DNA.

IRGB10 provides host protection against infection with *A.f in vivo*.

We previously reported the crucial physiological role of inflammasomes in host defense during aspergillosis[17]. We therefore investigated the role of GBPs and IRGB10 in inflammasome-mediated antifungal responses during *A.f* infection. Both WT and *Gbp*$^{chr3-/-}$ mice showed similar susceptibility to *A.f* infection, and the mortality rate was less than 50% (Fig. 6a). However, the mortality rate was significantly increased in IRGB10-deficient mice and approximately 90% of *Irgb10*$^{-/-}$ mice succumbed to *A.f* infection (Fig. 6b). The lungs of mice lacking IRGB10 showed a higher extent of gross pathology and hemorrhage than did the lungs of WT mice (Fig. 6c). In addition, Gomori methenamine silver staining showed that *A.f* infection in mice lacking IRGB10 resulted in necrotizing invasive lesions whereas the infection in WT mice was largely restricted to airway lumens (Fig. 6d,e). The

lungs of infected *Irgb10*$^{-/-}$ mice showed transmural inflammation and necrosis of bronchioles, blood vessels and alveolar septa, with marked intravascular accumulation of inflammatory cells in affected areas but limited extravasation of predominantly histocytic (macrophages) inflammation (Fig. 6d,e). These necrotizing lesions in *Irgb10*$^{-/-}$ mice were also associated with interstitial and luminal hemorrhage, edema, and widespread vascular invasion by intact fungal hyphae (Fig. 6d,e yellow head arrows). In contrast, *A.f* infection in WT lungs was generally restricted to the lumens of terminal airways and adjacent alveoli, with lesions characterized by fungal hyphae surrounded by dense cellular exudates consisting of mixed degenerating and intact neutrophils and macrophages (Fig. 6d,e, yellow head arrows). These suppurative inflammatory exudates completely surrounded the fungal hyphae, which were often disrupted (Fig. 6d,e). Although there was limited necrosis of some bronchiolar epithelial cells in affected airways, there was no sign of transmural invasion or necrosis of alveoli, bronchioles, or blood vessels and interstitial hemorrhage and edema in WT lungs. These results collectively demonstrate that IRGB10 promotes more effective host immune responses to pulmonary *A.f* infection, which reduces mortality by preventing vascular invasion and dissemination of the infection. In line with the staining, we observed significantly higher *18S* rRNA level in the lungs of *Irgb10*$^{-/-}$ mice compared to WT mice (Fig. 6f). Consistent with our *in vitro* findings, caspase-1 cleavage and IL-1β release were impaired in the lungs of *Irgb10*$^{-/-}$ mice compared with WT mice. In contrast, concentration of the pro-inflammatory cytokine IL-6 was higher in *Irgb10*$^{-/-}$ mice (Fig. 6g,h). IRGB10 was required in both the stromal and hematopoietic compartments for protection during pulmonary aspergillosis, as previously observed in mice lacking both NLRP3 and AIM2[17] (Supplementary Fig. 9c). Similar to mice lacking inflammasome components[42], *Irgb10*$^{-/-}$ immunocompetent mice were not susceptible to *A.f* (Supplementary Fig. 9a,b). These results collectively demonstrate that IRGB10 mediates immune responses in the lungs, thereby restricting fungal dissemination and promoting host defense during aspergillosis via regulation of the inflammasomes.

DISCUSSION

In this study, we delineated how two distinct innate immune sensing pathways coordinatedly regulate the activation of inflammasomes upon *A.f* infection[17]. We identified that IRGB10, under the regulation of IRF1, plays a critical role in promoting inflammasome activation by releasing fungal ligands (Supplementary Fig. 10). During *C. albicans* infection, yeast PAMPs are recognized by TLR2 and Dectin-1 receptors to engage the NLRP3 inflammasome[16]. Dectin-1 and particularly Dectin-2 are also required for efficient activation of the NLRP3 inflammasome during *H. capsulatum infection*[43]. Although it is known that *A.f* exposes myriads of PAMPs recognized by TLR2, TLR3, TLR4, TLR9, and Dectin-1[4-6,8,44], whether these pattern recognition receptors engage the inflammasomes upon infection with *A.f* remained unclear. We determined the central role of these receptors in regulating inflammasome activation during *A.f*. We previously reported mice lacking components of inflammasomes are highly susceptible to *A.f* infection[17]. Futhermore, mice lacking TLR2, TLR3, TLR4 and Dectin-1 are susceptible to aspergillosis[4,12,13,22], which might be due to defective inflammasome activation (Supplementary Table 1).

Here, we show that downstream of TLRs and Dectin-1, their respective adaptors MyD88/TRIF and the SYK–CARD9–MALT1 complex are also required for optimal inflammasome activation in response to *A.f* (Supplementary Table 1). The CLR-SYK pathway, rather than the TLR-MyD88 axis, is predominantly involved in activation of ERK and NF-κB during sensing of fungal ligands[45,46]. Intriguingly, despite normal expression of IRF1 in the absence of TLR-mediated signaling through SYK-CARD9-MALT1, inflammasome activation is still reduced during *A.f* infection. Critically, our data suggested that TLR-mediated signaling is required for the activation of IRF1, revealing the mechanism by which the CLR and TLR pathways coordinately prime inflammasome activation during *A.f* infection.

Members of the IFN-inducible GTPase family, including GBPs and IRGB10, are known target genes of IRF1. GBPs and IRGB10 target the bacterial cell membrane, leading to release of bacterial ligands and subsequent inflammasome activation[24,25]. Although both GBPs and IRGB10 are induced in an IRF1-dependent manner upon *A.f* infection, only IRGB10 is required for inflammasome activation unlike in the case of bacterial infections, where both are necessary for optimal inflammasome activation[24-26]. These observations provide an excellent example of how the innate immune system tailors unique, pathogen-specific response using common regulator or effector proteins. In line with our findings, it has been shown that IRGB10 is necessary for optimal NLRP3 and AIM2 inflammasome activation during bacterial infection by facilitating release of LPS from *E. coli* and DNA from *F. novicida*[25]. IRGB10 possesses putative myristoylation motifs, transmembrane amphipathic helices and antimicrobial stretches that are involved in membrane attachment and permeabilization. Among these, we demonstrated that peptides derived from the antimicrobial stretches of IRGB10 inhibited fungal growth, induced hyphae damage and modified the *A.f* surface. We also showed that β-glucan, one of the major components of the fungal cell wall is able to directly activate inflammasomes. Thus, we propose a model in which IRGB10 targets fungal cell wall and facilitates release of ligands for inflammasome activation. However, which inflammasome (NLRP3 or AIM2) requires IRGB10 for its activation during *A.f* infection remains unknown. The residual activation of the NLRP3 inflammasome in *Irgb10*$^{-/-}$ cells was perhaps dependent on the potassium efflux caused by the growth of fungal hyphae. We also show that IRGB10 co-localizes with the fungal cell wall and inhibits hyphae growth, but the mechanism by which IRGB10 is recruited to the fungal cell wall and facilitates the release of ligands remains unclear. The specific component of the fungal cell wall targeted by IRGB10 is also not known and warrants further investigation.

In conclusion, our study revealed the molecular mechanisms by which innate immune sensors promote inflammasome activation during fungal infection and identified the transcription factor IRF1 and the GTPase IRGB10 as mediators of inflammasome activation during *A.f* infection.

METHODS

Mice.

Tlr2$^{-/-}$[48], *Tlr3*$^{-/-}$[49], *Tlr4*$^{-/-}$[50], *Tlr9*$^{-/-}$[51], *Myd88*$^{-/-}$[52], *Tirf*$^{-/-}$[53], *Dectin-1*$^{-/-}$[54], *Syk*$^{fl/fl}$*LysM*^{Cre}[55,56], *Card9*$^{-/-}$[57], *Malt1*$^{-/-}$[58], *Irf1*$^{-/-}$[59], *Gbp*$^{chr3-/-}$[60], *Irgb10*$^{-/-}$[25], and *Nlrp3*$^{-/-}$*Aim2*$^{-/-}$[17] mice were generated as described previously. All mice were backcrossed to the C57BL/6 background. Mice were bred at St. Jude Children's Research Hospital (St. Jude). Animal studies were conducted under protocols approved by the St. Jude Animal Care and Use Committee.

Aspergillus strain and culture.

Aspergillus fumigatus (A.f) A1160 strain was grown on 2% (w/v) malt/2% (w/v) agar slants for 1 week. Conidia were harvested in water containing 0.1% (v/v) Tween-20[61].

In vitro stimulation of GM-CSF–derived BMDMs.

Granulocyte macrophage colony-stimulating factor (GM-CSF)-derived bone marrow cells (denoted as BMDMs) were prepared as previously described[62]. In brief, bone marrow cells were grown in RPMI (10-040-CV, Corning cellgro™) supplemented with 10% FBS (TMS-013-B, lot number QVP1404280, Millipore, Billerica, MA or S1620, lot number 221C16, BioWest, Riverside, MO), 1% penicillin–streptomycin, 1% non-essential amino acids, 1% sodium pyruvate, 0.1% β-mercaptoethanol, and 20 ng/mL GM-CSF for 7 days. BMDMs (3×10^6) were seeded in 12-well cell culture plates (3513, Costar) in DMEM (11995-065, Gibco) supplemented with 10% FBS and 1% penicillin–streptomycin and infected with *A. fumigatus* conidia at a multiplicity of infection (MOI) of 20 for 20 h. For priming, BMDMs were incubated with 100 ng/mL of LPS (tlrl-smlps, Invivogen) or 25 μg/mL of curdlan (C7821, Sigma) for 3 h and washed before infecting with *A. fumigatus* as described above. For polysaccharide transfection, 20 μg curdlan from Alcaligenes faecalis (C7821, Sigma) was resuspended in PBS and mixed with Xfect™ (631318, Takara,) as per the manufacturer's protocol. The reaction mixture was added to BMDMs in Opti-MEM (31985-070, ThermoFisher Scientific).

In vitro isolation and culture and infection of lung fibroblasts.

Lung fibroblasts (LFs) were prepared from mouse lungs as previously described[63]. Briefly, the lungs were harvested, cut into small pieces, and suspended in 0.25% trypsin lysis buffer (25200-056, Gibco) for 30 min at 37°C under agitation. LF medium, composed of DMEM, 10% FBS, 1% penicillin–streptomycin, 1% nonessential amino acids, 1% sodium pyruvate, 1% HEPES buffer, 1% L-glutamine, and 0.25% β-mercaptoethanol, was added to the suspension. Cell suspensions were centrifuged at 1500 rpm for 5 min, and pellets were resuspended in LF medium and plated onto culture dishes.

In vivo A. fumigatus infection.

The sample size for *in vivo* was constrained by availability of animals. Mice were selected based on age and sex. *In vivo* experiments used male and female mice that were 7 to 8 weeks of age. Mice were infected with *A. fumigatus* as previously described[64]. Briefly,

cyclophosphamide monohydrate (C0768, Sigma) was dissolved in sterile PBS and administered intraperitoneally (150 mg per kg of body weight). Cortisone 21-acetate (C3130, Sigma) was suspended in 0.1% Tween 20 in PBS and subcutaneously injected (112 mg per kg of body weight). Mice were given a combination of cyclophosphamide and cortisone acetate 2 days before infection and on the day of infection for the immunocompromised model of pulmonary aspergillosis or directly infected without cyclophosphamide and cortisone acetate treatment for the immunocompetent model. Mice were anesthetized by isoflurane inhalation and inoculated intranasally with 5.5×10^5 conidia of *A. fumigatus* in 30 μL of 0.1% Tween 20 in PBS for the immunocompromised model or 10^7 conidia of *A. fumigatus* in 50 μL 0.1% Tween 20 in PBS for the immunocompetent model. Fungal burden was quantified by RT-PCR as previously described[22].

Bone Marrow Chimeras.

Mice were subjected to a single dose of irradiation (1,000 rad). Mice were retroorbitally injected with 10^7 bone marrow cells from the femur and tibia of donor mice 2 h after irradiation. The reconstitution rate was evaluated 6 weeks after bone marrow transfer by flow staining of CD45.1 and CD45.2 in blood leukocytes, which was at least 95%. Mice were infected as described above 6 weeks post bone marrow transfer.

Immunoblotting analysis.

To check for caspase-1 cleavage by western blot analysis, cells and supernatants were lysed in caspase lysis buffer and sample loading buffer containing SDS and 100 mM dithiothreitol. To check for signaling molecules, BMDMs were lysed in 1× RIPA buffer and sample loading buffer as described previously[17]. For IRF1 nuclear localization experiments, this was followed by nuclear/cytoplasmic protein extraction with the NE-PER™ Kit (78835, ThermoFisher Scientific) according to the manufacturer's protocol. Lung tissues were homogenized in PBS containing protease inhibitors (Roche). Homogenates were then mixed in a 1:1 ratio with 2× RIPA buffer, and protein concentrations were determined and diluted to 1 μg/μL with the sample loading buffer. Proteins (15 μg) were separated on 8%–10% or 12% polyacrylamide gels. After electrophoretic transfer of protein onto PVDF membranes (Millipore), membranes were blocked in 5% skim milk and incubated with primary antibodies against caspase-1 (AG-20B-0042, Adipogen), caspase-1 p10 (sc-515,santa cruz), Irf1 (D5E4, Cell Signaling), GBP2 (11854-1-AP, Proteintech), GBP5 (13220-1-AP, Proteintech), IRGB10[65], p-IκBα (2859, Cell Signaling), t-IκBα (9242, Cell Signaling), p-ERK (9101, Cell Signaling), t-ERK (9102, Cell Signaling), t-SYK (2712, Cell Signaling), MyD88 (D80F5, Cell Signaling), NLRP3 (AG-20B-0006, Adipogen), LaminB (sc6216, Santa Cruz Biotechnology), GAPDH (D16h11, Cell Signaling) or Actin (8H10D10, Cell Signaling), followed by secondary anti-rabbit, anti-mouse, or anti-goat HRP antibodies (Jackson ImmunoResearch Laboratories). Membranes were developed with an Amersham imager and analyzed with Fiji[66].

MyD88 overexpression.

L929 cells were transfected with pFLAG-CMV-2-MyD88 (plasmid with MyD88 construct) or pFLAG-CMV-2 (empty plasmid) as control with Xfect™ (631318, Takara,) as per the manufacturer's protocol. 24 h post transfection, cells were infected with 20 MOI *A.*

fumigatus resting conidia for the indicated time points (0, 2, 4, and 8 h). This was followed by nuclear/cytoplasmic protein extraction with the NE-PER™ Kit (78835, ThermoFisher Scientific) according to the manufacturer's protocol. Protein concentration was measured with Pierce™ BCA Protein Assay Kit (23227, ThermoFisher Scientific). Then, 10 μg of protein lysate was loaded for immunoblotting analysis as mentioned before.

mCherry-Irgb10 lentiviral expression.

The N-terminal mCherry-IRGB10 fusion construct was constructed using the NEBuilder HiFi DNA assembly kit (E2621S, New England BioLabs) according to the manufacturer's protocol. PCR products were generated for mCherry (5'-AGAAGATTCTAGAGCTAGCGATGGTGAGCAAGGGCGAG-3') and (5'-CTTGTACAGCTCGTCCATGCC-3') and Irgb10 (5'-GGCATGGACGAGCTGTACAAGATGGGTCAGTCTTCTTCTAAAC-3') and (5'-GCGGATCCGATTTAAATTCGTTACTCAGAGTCCACACTGTC-3')and the vector backbone pCDH-CMV-MCS-EF1a-GFP-Neo (modified from CD516B-2, System Biosciences) was digested by EcoRI and treated with phosphatase to prevent re-ligation. To generate lentiviral particles, plasmids psPAX2 (12260, Addgene), pMD2.G (12259, Addgene), and the mCherry-IRGBIO containing transfer plasmid were co-transfected into 293T cells. Viral particle-containing supernatant plus polybrene (6 μg/mL) was used to transduce *Irgb10*$^{-/-}$ primary mouse fibroblasts. Transduced cells were selected with G418 (400 μg/mL, A1720, Sigma-Aldrich) to generate fibroblasts expressing mCherry-tagged IRGB10.

Real-time qRT-PCR analysis.

RNA was extracted using TRIzol (15596026, ThermoFisher Scientific) and converted into cDNA by using the High-Capacity cDNA Reverse Transcription Kit (4368814, Applied Biosystems). Real-time qPCR was performed on an ABI 7500 real-time PCR instrument with 2× SYBR Green (4368706, Applied Biosystems). Real-time qRT-PCR sequences used for the study are described in Supplementary Table 2.

Phagocytosis and Conidiocidal Assays.

Phagocytosing ability per BMDM was determined by calculating the number of BMDMs that had one or more conidia phagocytosed after 1 h of infection with 10 MOI of *A. fumigatus* resting conidia. The conidiocidal activity of IRGB10 peptides was calculated by infecting BMDMs with 1 MOI of resting conidia and incubating with the corresponding concentration of IRGB10 peptides for 5 h. Following this, cells were lyzed with 0.1 % triton X100, plated on LB petri dishes and the number of colony forming units were counted.

Peptide susceptibility assay.

The susceptibility of *A. fumigatus* to IRGB10 peptides was undertaken by measuring the minimal inhibitory concentration of each peptide in 96-well flat bottom plates, as previously described[67].

Hyphae damage assay (XTT assay).

The susceptibility of *A. fumigatus* to BMDMs and IRGB10 peptides were determined using the protocol described in Shepardson *et al*[68], and *Loures and Levitz*[69].

Cytokine analysis.

Cytokine levels were determined by multiplex ELISA (MCYTOMAG-70K, Millipore) according to the manufacturer's instructions.

Immunofluorescence staining.

For immunofluorescence staining, BMDMs (1×10^6) or LFs (1×10^5) were seeded on 4-well, 15-μm slides (80426, ibidi), in DMEM supplemented with 10% FBS and 1% penicillin–streptomycin and infected with *A. fumigatus* conidia with 20 MOI for the indicated time. Cells were washed 3 times and fixed in 4% paraformaldehyde for 15 min at room temperature, followed by blocking in PBS containing 10% goat serum (PCN5000, Life Technologies) supplemented with 0.2% saponin (47036, Sigma–Aldrich) for 1 h at room temperature. IRGB10 was stained using an affinity-purified polyclonal rabbit anti-IRGB10 antibody (1:1000 dilution) overnight at 4°C[65]. The antibody was further purified by pre-absorption with cell lysates from IFN-γ–stimulated *Irgb10*$^{-/-}$ BMDMs. Next, cells were washed 4 times with PBS and stained with an anti-rabbit secondary Alexa Fluor 568 antibody (1:250 dilution, A11036, Invitrogen) in PBS containing 10% goat serum supplemented with 0.2% saponin for 1 h at room temperature. The *A. fumigatus* cell wall was stained with PBS supplemented with 10 μg/mL calcofluor white (18909, Sigma) for 1 h at room temperature. Cells were visualized and imaged using a Nikon C2 confocal microscope, and super-resolved 3-dimensional images were taken on a Zeiss Elyra PS.1 microscope using the structured illumination microscopy technique. Pictures were analyzed and aligned by Imaris (Bitplane's core scientific software).

Scanning Electron microscopy.

A. fumigatus was pre-grown 16 h before incubation with IRGB10 peptides for 5 h. Coverslips were fixed in a mixture of 2.5% glutaraldehyde (Electron Microscopy Sciences, Hatfield, Pennsylvania, USA, #16200), 2% paraformaldehyde (EMS #15700) in 0.1 M sodium cacodylate buffer (pH 7.4) (EMS #12310). Samples were then rinsed in 0.1 M sodium cacodylate buffer four times for five minutes each, followed by a secondary fixation in 1% osmium tetroxide (#19140) in ultrapure water for 60 minutes. The samples were then rinsed four times in ultrapure water for five minutes each, followed by dehydration in a graded ethanol series (30%, 50%, 70%, 90%, 100% ×2) for ten minutes each step. The coverslips were then loaded into a critical point drier (Autosamdri 931.GL, Tousimis, Maryland, USA) which was set to perform multiple liquid CO_2 exchanges in three ten-minute 'purge' cycles with Stasis mode. Once dried, the coverslips were mounted on aluminum stubs using conductive carbon adhesive tabs (EMS #77825-06), with the edges being painted with conductive silver paint (Ted Pella, Redding, California, USA, #16062) to reduce charging, and sputter coated with ~8nm of iridium (Desk V, Denton Vacuum, New Jersey, USA). The samples were then loaded into the Teneo VS SEM (FEI-Thermo Fisher, Hillsboro, Oregon, USA) and imaged.

Amino acid sequence analysis.

Putative antimicrobial regions in IRGB10 amino acid sequence were predicted using AMPA algorithm with 0.25 of threshold[70]. Next, the homologue sequences of IRG family members were analyzed with iAMPpred to confirm the antimicrobial (antifungal, antibacterial and antiviral) activity[71]. Conservation at each residue position of the predicted antimicrobial strech was graphically plotted using WebLogo3[72].

Peptide biosynthesis.

IRGB10 peptides (1, 2, 3 and scrambles, Supplementary Table. 3) were synthesized in the Hartwell Center of St. Jude Children's Research Hospital using standard Fmoc chemistry on a Protein Technologies Symphony X instrument. Following synthesis, peptides were cleaved off the resin using TFA/Water/Thioanisole/TIS/Phenol/EDT and precipitated in ice cold diethyl ether. After centrifugation, peptides were dissolved in water and lyophilized. HPLC analysis was performed on a Waters Alliance 2695 separation module and mass spectrometry was recorded using MALDI on a Bruker Microflex instrument. HPLC purification was performed on a Waters Preparative HPLC system.

Statistical analysis.

GraphPad Prism 7.0 was used for data analysis. Data are represented as mean ± standard error of the mean. Statistical significance was determined by a log-rank test. $P < 0.05$ was considered statistically significant. The exact *P*-values are represented in the Supplementary Table 3.

Supplementary Material

Refer to Web version on PubMed Central for supplementary material.

Acknowledgements

We thank members of the Kanneganti lab, the St. Jude Children's Hospital Veterinary Pathology Core, Macromolecular Synthesis Core and Electron Microscopy Core. Images were acquired at the SJCRH Cell & Tissue Imaging Center, which is supported by SJCRH and NCI P30 CA021765-35. Work from our laboratories is supported by the US NIH (AM01935, AI124346, AR056296, and CA163507 to T.-D.K.) and the American Lebanese Syrian Associated Charities (to T.-D.K.). Masahiro Yamamoto is supported by the Research Program on Emerging and Re-emerging Infectious Diseases (18fk0108047h0002) and Japanese Initiative for Progress of Research on Infectious Diseases for global Epidemic (18fm0208018h0002) from Agency for Medical Research and Development (AMED).

Abbreviations:

A.f	A. fumigatus, Aspergillus fumigatus
AIM2	Absent in melanoma 2
ALRs	AIM2-like receptors
ASC	Apoptosis-associated speck-like protein containing a CARD
Bcl10	B-cell lymphoma/leukemia 10

CARD9	Caspase recruitment domain–containing protein 9
CLR	C-type lectin receptor
ERK	Extracellular signal-regulated kinase
GBP	Guanylate binding protein
GMS	Gomori methenamine silver
IκBα	nuclear factor of kappa light polypeptide gene enhancer in B-cells inhibitor, alpha
IRF1	Interferon regulatory factor 1
IRGB10	Immunity-related guanosine triphosphatase family member b10
IRES	Internal ribosome entry site
LPS	Lipopolysaccharide
MALT1	Mucosa-associated lymphoid tissue lymphoma translocation protein 1
MAPK	Mitogen-activated protein kinase
MyD88	Myeloid differentiation primary response 88
NF-κB	Nuclear factor kappa-light-chain enhancer of activated B cells
NLRs	nucleotide-binding oligomerization domain–like receptors, leucine-rich repeat containing family
NLRP3	nucleotide-binding oligomerization domain, leucine-rich repeat and pyrin domain–containing 3
PAMP	Pathogen-associated molecular pattern
SYK	Spleen tyrosine kinase
TLRs	Toll-like receptors
TRIF	Toll/interleukin-1 receptor domain-containing adaptor protein inducing interferon beta
WT	wild type

REFERENCES

1. Dagenais TRT & Keller NP Pathogenesis of Aspergillus fumigatus in Invasive Aspergillosis. Clin. Microbiol. Rev 22, 447–465 (2009). [PubMed: 19597008]
2. Latgé J-P Aspergillus fumigatus and Aspergillosis. Clin. Microbiol. Rev 12, 310–350 (1999). [PubMed: 10194462]
3. Segal BH Aspergillosis. N. Engl. J. Med. 360, 1870–1884 (2009). [PubMed: 19403905]

4. Carvalho A et al. TLR3 essentially promotes protective class I—restricted memory CD8+ T-cell responses to Aspergillus fumigatus in hematopoietic transplanted patients. Blood 119, 967–977 (2012). [PubMed: 22147891]
5. Chai LYA et al. Modulation of Toll-Like Receptor 2 (TLR2) and TLR4 Responses by Aspergillus fumigatus. Infect. Immun 77, 2184–2192 (2009). [PubMed: 19204090]
6. Kasperkovitz PV, Cardenas ML & Vyas JM TLR9 Is Actively Recruited to *Aspergillusfumigatus* Phagosomes and Requires the N-Terminal Proteolytic Cleavage Domain for Proper Intracellular Trafficking. J. Immunol 185, 7614–7622 (2010). [PubMed: 21059889]
7. Loures FV et al. Recognition of Aspergillus fumigatus Hyphae by Human Plasmacytoid Dendritic Cells Is Mediated by Dectin-2 and Results in Formation of Extracellular Traps. PLOS Pathog. 11, e1004643 (2015). [PubMed: 25659141]
8. Meier A et al. Toll-like receptor (TLR) 2 and TLR4 are essential for Aspergillus-induced activation of murine macrophages. Cell. Microbiol 5, 561–570 (2003). [PubMed: 12864815]
9. Netea MG et al. Aspergillus fumigatus Evades Immune Recognition during Germination through Loss of Toll-Like Receptor-4-Mediated Signal Transduction. J. Infect. Dis 188, 320–326 (2003). [PubMed: 12854089]
10. Ramaprakash H, Ito T, Standiford TJ, Kunkel SL & Hogaboam CM Toll-Like Receptor 9 Modulates Immune Responses to Aspergillus fumigatus Conidia in Immunodeficient and Allergic Mice. Infect. Immun 77, 108–119 (2009). [PubMed: 18936185]
11. Serrano-Gómez D, Leal JA & Corbí AL DC-SIGN mediates the binding of Aspergillus fumigatus and keratinophylic fungi by human dendritic cells. Immunobiology 210, 175–183 (2005). [PubMed: 16164024]
12. Balloy V et al. Involvement of Toll-Like Receptor 2 in Experimental Invasive Pulmonary Aspergillosis. Infect. Immun 73, 5420–5425 (2005). [PubMed: 16113258]
13. Bellocchio S et al. The Contribution of the Toll-Like/IL-1 Receptor Superfamily to Innate and Adaptive Immunity to Fungal Pathogens In Vivo. J. Immunol 172, 3059–3069 (2004). [PubMed: 14978111]
14. Gringhuis SI et al. Dectin-1 is an extracellular pathogen sensor for the induction and processing of IL-1β via a noncanonical caspase-8 inflammasome. Nat. Immunol. 13, 246–254 (2012). [PubMed: 22267217]
15. Gross O et al. Syk kinase signalling couples to the Nlrp3 inflammasome for antifungal host defence. Nature 459, 433–436 (2009). [PubMed: 19339971]
16. Hise AG et al. An Essential Role for the NLRP3 Inflammasome in Host Defense against the Human Fungal Pathogen Candida albicans. Cell Host Microbe 5, 487–497 (2009). [PubMed: 19454352]
17. Karki R et al. Concerted Activation of the AIM2 and NLRP3 Inflammasomes Orchestrates Host Protection against Aspergillus Infection. Cell Host Microbe 17, 357–368 (2015). [PubMed: 25704009]
18. Lei G et al. Biofilm from a clinical strain of Cryptococcus neoformans activates the NLRP3 inflammasome. Cell Res. 23, 965–968 (2013). [PubMed: 23567555]
19. Saïïd-Sadier N, Padilla E, Langsley G & Ojcius DM Aspergillus fumigatus Stimulates the NLRP3 Inflammasome through a Pathway Requiring ROS Production and the Syk Tyrosine Kinase. PLoS ONE 5, e10008 (2010). [PubMed: 20368800]
20. Tavares AH et al. NLRP3 Inflammasome Activation by Paracoccidioides brasiliensis. PLoS Negl. Trop. Dis 7, e2595 (2013). [PubMed: 24340123]
21. Triantafilou M, Hughes TR, Morgan BP & Triantafilou K Complementing the inflammasome. Immunology 152–164 (2015). doi:10.1111/imm.l2556
22. Werner JL et al. Requisite role for the Dectin-1 beta-glucan receptor in pulmonary defense against Aspergillus fumigatus. J. Immunol. Baltim. Md 1950 182, 4938–4946 (2009).
23. Man SM, Karki R & Kanneganti T-D Molecular mechanisms and functions of pyroptosis, inflammatory caspases and inflammasomes in infectious diseases. Immunol. Rev 277, 61–75 (2017). [PubMed: 28462526]

24. Man SM et al. The transcription factor IRF1 and guanylate-binding proteins target activation of the AIM2 inflammasome by Francisella infection. Nat. Immunol 16, 467–475 (2015). [PubMed: 25774715]
25. Man SM et al. IRGB10 Liberates Bacterial Ligands for Sensing by the AIM2 and Caspase-11-NLRP3 Inflammasomes. Cell 167, 382–396.e17 (2016). [PubMed: 27693356]
26. Meunier E et al. Guanylate-binding proteins promote activation of the AIM2 inflammasome during infection with Francisella novicida. Nat. Immunol 16, 476–484 (2015). [PubMed: 25774716]
27. Rathinam VAK et al. TRIF licenses caspase-11-dependent NLRP3 inflammasome activation by gram-negative bacteria. Cell 150, 606–619 (2012). [PubMed: 22819539]
28. Mambula SS, Sau K, Henneke P, Golenbock DT & Levitz SM Toll-like Receptor (TLR) Signaling in Response to Aspergillus fumigatus. J. Biol. Chem 277, 39320–39326 (2002). [PubMed: 12171914]
29. Wang JE et al. Involvement of CD14 and toll-like receptors in activation of human monocytes by Aspergillus fumigatus hyphae. Infect. Immun 69, 2402–2406 (2001). [PubMed: 11254600]
30. Ramirez-Ortiz ZG et al. Toll-like receptor 9-dependent immune activation by unmethylated CpG motifs in Aspergillus fumigatus DNA. Infect. Immun. 76, 2123–2129 (2008). [PubMed: 18332208]
31. Hohl TM et al. Aspergillus fumigatus triggers inflammatory responses by stage-specific beta-glucan display. PLoS Pathog. 1, e30 (2005). [PubMed: 16304610]
32. Steele C et al. The Beta-Glucan Receptor Dectin-1 Recognizes Specific Morphologies of Aspergillus fumigatus. PLOS Pathog. 1, e42 (2005). [PubMed: 16344862]
33. Plato A, Hardison SE & Brown GD Pattern recognition receptors in antifungal immunity. Semin. Immunopathol 37, 97–106 (2015). [PubMed: 25420452]
34. Bretz C et al. MyD88 Signaling Contributes to Early Pulmonary Responses to Aspergillus fumigatus. Infect. Immun 76, 952–958 (2008). [PubMed: 18039832]
35. Wevers BA et al. Fungal Engagement of the C-Type Lectin Mincle Suppresses Dectin-1-Induced Antifungal Immunity. Cell Host Microbe 15, 494–505 (2014). [PubMed: 24721577]
36. Feng H et al. NLRX1 promotes immediate IRF1-directed antiviral responses by limiting dsRNA-activated translational inhibition mediated by PKR. Nat. Immunol **advance online publication,** (2017).
37. Negishi H et al. Evidence for licensing of IFN-γ-induced IFN regulatory factor 1 transcription factor by MyD88 in Toll-like receptor-dependent gene induction program. Proc. Natl. Acad. Sci 103, 15136–15141 (2006). [PubMed: 17018642]
38. Man SM, Place DE, Kuriakose T & Kanneganti T-D Interferon-inducible guanylate-binding proteins at the interface of cell-autonomous immunity and inflammasome activation. J. Leukoc. Biol 101, 143–150 (2017). [PubMed: 27418355]
39. Kim B-H, Shenoy AR, Kumar P, Bradfield CJ & MacMicking JD IFN-inducible GTPases in Host Defense. Cell Host Microbe 12, 432–444 (2012). [PubMed: 23084913]
40. Kim B-H et al. Interferon-induced guanylate-binding proteins in inflammasome activation and host defense. Nat. Immunol 17, 481–489 (2016). [PubMed: 27092805]
41. Heinekamp T et al. Interference of Aspergillus fumigatus with the immune response. Semin. Immunopathol 37, 141–152 (2015). [PubMed: 25404120]
42. Caffrey AK et al. IL-1α Signaling Is Critical for Leukocyte Recruitment after Pulmonary Aspergillus fumigatus Challenge. PLoS Pathog. 11, (2015).
43. Chang T-H et al. Dectin-2 is a primary receptor for NLRP3 inflammasome activation in dendritic cell response to Histoplasma capsulatum. PLOS Pathog. 13, e1006485 (2017). [PubMed: 28671985]
44. Drummond RA & Brown GD The role of Dectin-1 in the host defence against fungal infections. Curr. Opin. Microbiol 14, 392–399 (2011). [PubMed: 21803640]
45. Geijtenbeek TBH & Gringhuis SI Signalling through C-type lectin receptors: shaping immune responses. Nat. Rev. Immunol 9, 465–479 (2009). [PubMed: 19521399]
46. Slack EC et al. Syk-dependent ERK activation regulates IL-2 and IL-10 production by DC stimulated with zymosan. Eur. J. Immunol 37, 1600–1612 (2007). [PubMed: 17458858]

47. Kuriakose T, Zheng M, Neale G & Kanneganti T-D IRF1 Is a Transcriptional Regulator of ZBP1 Promoting NLRP3 Inflammasome Activation and Cell Death during Influenza Virus Infection. J. Immunol 200, 1489–1495 (2018). [PubMed: 29321274]
48. Takeuchi O, Hoshino K & Akira S Cutting Edge: TLR2-Deficient and MyD88-Deficient Mice Are Highly Susceptible to Staphylococcus aureus Infection. J. Immunol 165, 5392–5396 (2000). [PubMed: 11067888]
49. Alexopoulou L, Holt AC, Medzhitov R & Flavell RA Recognition of double-stranded RNA and activation of NF-κB by Toll-like receptor 3. Nature 413, 35099560 (2001).
50. Hoshino K et al. Cutting edge: Toll-like receptor 4 (TLR4)-deficient mice are hyporesponsive to lipopolysaccharide: evidence for TLR4 as the Lps gene product. J. Immunol. Baltim. Md 1950 162, 3749–3752 (1999).
51. Hemmi H et al. A Toll-like receptor recognizes bacterial DNA. Nature 408, 35047123 (2000).
52. Kawai T, Adachi O, Ogawa T, Takeda K & Akira S Unresponsiveness of MyD88-deficient mice to endotoxin. Immunity 11, 115–122 (1999). [PubMed: 10435584]
53. Yamamoto M et al. Role of Adaptor TRIF in the MyD88-Independent Toll-Like Receptor Signaling Pathway. Science 301, 640–643 (2003). [PubMed: 12855817]
54. Marakalala MJ et al. Differential Adaptation of Candida albicans In Vivo Modulates Immune Recognition by Dectin-1. PLOS Pathog. 9, e1003315 (2013). [PubMed: 23637604]
55. Saijo K et al. Essential role of Src-family protein tyrosine kinases in NF-KB activation during B cell development. Nat. Immunol 4, ni893 (2003).
56. Gurung P et al. Tyrosine Kinase SYK Licenses MyD88 Adaptor Protein to Instigate IL-1α-Mediated Inflammatory Disease. Immunity 46, 635–648 (2017). [PubMed: 28410990]
57. Gross O et al. Card9 controls a non-TLR signalling pathway for innate anti-fungal immunity. Nature 442, 651–656 (2006). [PubMed: 16862125]
58. Ruland J, Duncan GS, Wakeham A & Mak TW Differential requirement for Malt1 in T and B cell antigen receptor signaling. Immunity 19, 749–758 (2003). [PubMed: 14614861]
59. Matsuyama T et al. Targeted disruption of IRF-1 or IRF-2 results in abnormal type I IFN gene induction and aberrant lymphocyte development. Cell 75, 83–97 (1993). [PubMed: 8402903]
60. Yamamoto M et al. A cluster of interferon-γ-inducible p65 GTPases plays a critical role in host defense against Toxoplasma gondii. Immunity 37, 302–313 (2012). [PubMed: 22795875]
61. da Silva Ferreira ME et al. The akuB(KU80) mutant deficient for nonhomologous end joining is a powerful tool for analyzing pathogenicity in Aspergillus fumigatus. Eukaryot. Cell 5, 207–211 (2006). [PubMed: 16400184]
62. Lamkanfi M, Malireddi RKS & Kanneganti T-D Fungal Zymosan and Mannan Activate the Cryopyrin Inflammasome. J. Biol. Chem 284, 20574–20581 (2009). [PubMed: 19509280]
63. Tzeng T-C et al. A Fluorescent Reporter Mouse for Inflammasome Assembly Demonstrates an Important Role for Cell-Bound and Free ASC Specks during In Vivo Infection. Cell Rep. 16, 571–582 (2016). [PubMed: 27346360]
64. Man SM et al. Differential roles of caspase-1 and caspase-11 in infection and inflammation. Sci. Rep 7, srep45126 (2017).
65. Coers J et al. Chlamydia muridarum Evades Growth Restriction by the IFN-γ-Inducible Host Resistance Factor Irgb10. J. Immunol 180, 6237–6245 (2008). [PubMed: 18424746]
66. Schindelin J et al. Fiji: an open-source platform for biological-image analysis. Nat. Methods 9, 676–682 (2012). [PubMed: 22743772]
67. Briard B et al. Dirhamnolipids secreted from *Pseudomonas aeruginosa* modify anjpegungal susceptibility of *Aspergillus fumigatus* by inhibiting β1,3 glucan synthase activity. ISME J. 11, 1578–1591 (2017). [PubMed: 28338676]
68. Shepardson KM et al. Hypoxia enhances innate immune activation to Aspergillus fumigatus through cell wall modulation. Microbes Infect. 15, 259–269 (2013). [PubMed: 23220005]
69. Loures FV & Levitz SM XTT Assay of Antifungal Activity. Bio-Protoc. 5, (2015).
70. Torrent M et al. AMPA: an automated web server for prediction of protein antimicrobial regions. Bioinformatics 28, 130–131 (2012). [PubMed: 22053077]

71. Meher PK, Sahu TK, Saini V & Rao AR Predicting antimicrobial peptides with improved accuracy by incorporating the compositional, physico-chemical and structural features into Chou's general PseAAC. Sci. Rep 7, (2017).

72. Crooks GE, Hon G, Chandonia J-M & Brenner SE WebLogo: A Sequence Logo Generator. Genome Res. 14, 1188–1190 (2004). [PubMed: 15173120]

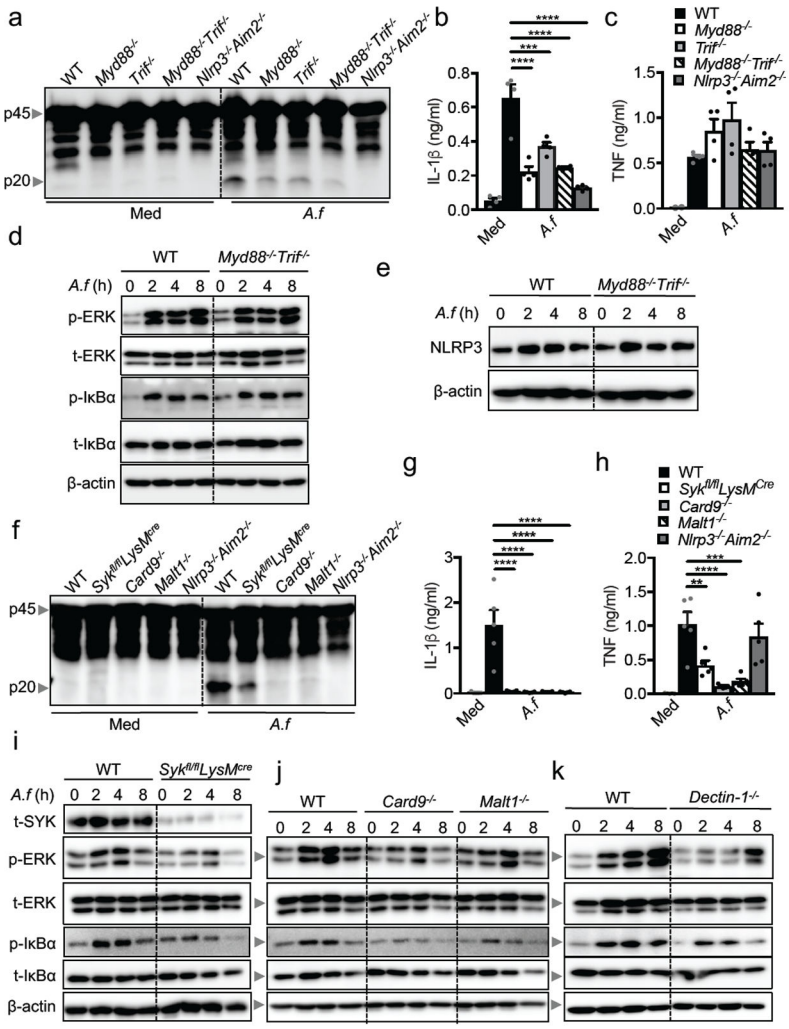

Figure 1. Downstream adaptors of TLRs and CLRs are required for inflammasome activation during *A. fumigatus* infection.

(**a**) Immunoblot analysis of pro-caspase-1 (p45) and the caspase-1 subunit p20 (p20) of unprimed BMDMs left untreated (medium alone [Med]) or assessed 20 h after infection with live *A. fumigatus* (*A.f*) resting conidia (multiplicity of infection [MOI], 20). (**b**) Release of IL-1β and (**c**) TNF in unprimed BMDMs left uninfected (Med) or assessed after 20 h with *A.f* (MOI, 20), $n = 4$ biologically independent samples, (**d**) Immunoblot analysis of phospho and total-ERK1/2 (p-ERK, t-ERK) or phospho- and total-IκBα (p-IκBα, t-IκBα) in unprimed WT and $Myd88^{-/-}Trif^{-/-}$ BMDMs 0–8 h after infection with live *A.f* resting conidia (MOI, 20). (**e**) Immunoblot analysis of NLRP3 in unprimed BMDMs 0–8 h after infection with *A.f* (MOI, 20). (**f**) Immunoblot analysis of caspase-1 (as in Fig. 1a), (**g**) release of IL-1β and (**h**) TNF in unprimed BMDMs left uninfected (Med) or assessed after 20 h with *A.f* (MOI, 20), $n = 5$ biologically independent samples. (**i,j,k**) Immunoblot analysis of p-, t-ERK and p-, t-IκBα in unprimed WT, $Syk^{fl/fl}LysM^{Cre}$, $Card9^{-/-}$, and $Malt1^{-/-}$ BMDMs 0–8 h after infection with live *A.f* resting conidia (MOI, 20). (**b,c,g,h**) $*P < 0.05$, $**P < 0.01$, $***P < 0.001$, and $****P < 0.0001$ (one-way ANOVA with Dunnett's multiple-comparisons test). Data are representative of (**a–k**) at least 3 independent

experiments (mean ± s.e.m.). The exact *P*-values are represented in the Supplementary Table 3.

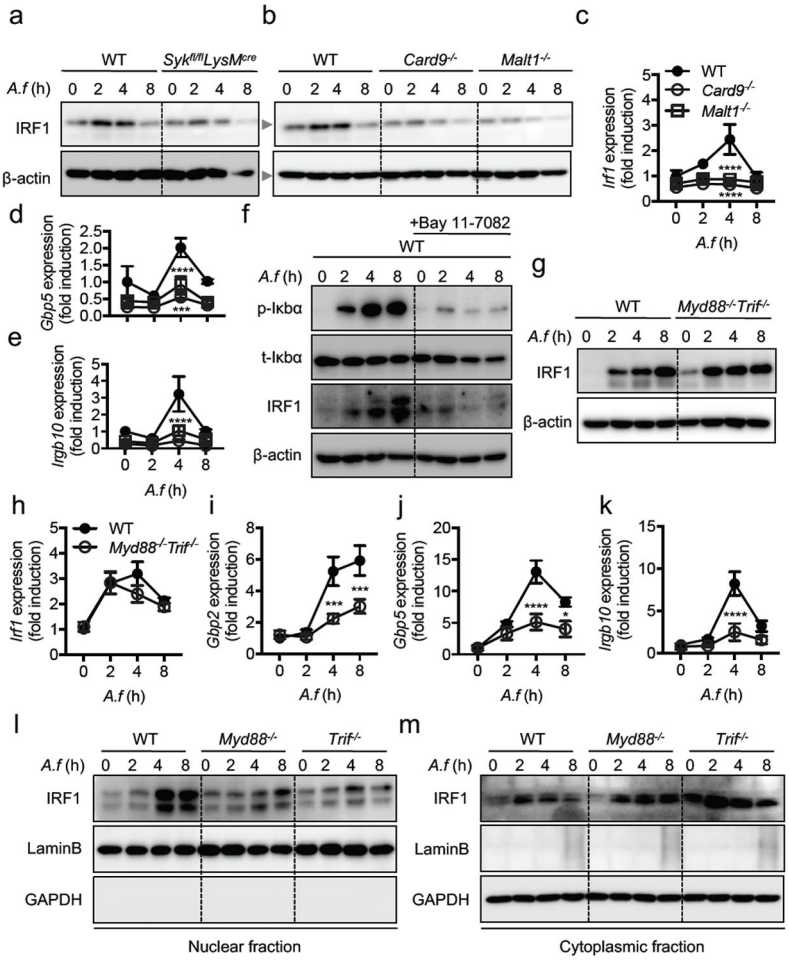

Figure 2. The SYK-CARD9-MALT1 complex regulates IRF1 expression, whereas the activation of IRF1 is MyD88/TRIF dependent.

(**a,b**) Immunoblot analysis of IRF1 in unprimed WT, *Syk*$^{fl/fl}$*LysM*^{Cre}, *Card9*$^{-/-}$, and *Malt1*$^{-/-}$ BMDMs 0–8 h after infection with live *A.f* resting conidia (MOI, 20). (**c,d,e**) Real-time quantitative RT-PCR analysis of *Ifr1*, *Gbp5* and *Irgb10* genes in WT, *Card9*$^{-/-}$ and *Malt1*$^{-/-}$ BMDMs 0–8 h after infection with *A.f* presented relative to that of the gene encoding β-actin. (**f**) Immunoblot analysis of p-, t-IκBα and IRF1 expression in unprimed WT BMDMs and WT BMDMs incubated with NF-κB inhibitor Bay 11-7082. (**g**) Immunoblot analysis of IRF1 in unprimed WT and *Myd88*$^{-/-}$ *Trif*$^{-/-}$ BMDMs 0–8 h after infection with live *A.f* resting conidia (MOI, 20). (**h,i,j,k**) Real-time quantitative RT-PCR analysis of *Ifr1*, *Gbp2*, *Gbp5*, and *Irgb10* genes in WT and *Myd88*$^{-/-}$ *Trif*$^{-/-}$ BMDMs 0–8 h after infection with *A.f* presented relative to that of the gene encoding β-actin. (**I,m**) Immunoblot analysis of IRF1 (top lanes), LaminB (middle lanes, nuclear fraction loading control), and GAPDH (bottom lanes, cytoplasmic fraction loading control) in unprimed (**I**) nuclear fraction and (**m**) cytoplasmic fraction of BMDMs 0–8 h after infection with *A.f* (MOI, 20). **P* < 0.05, ***P* < 0.01, ****P* < 0.001, and *****P* < 0.0001 (one-way ANOVA with Sidak's multiple-comparisons test), ****(**a–m**) Data are representative of at least 3 independent experiments (mean ± s.e.m.). The exact *P*-values are represented in the Supplementary Table 3.

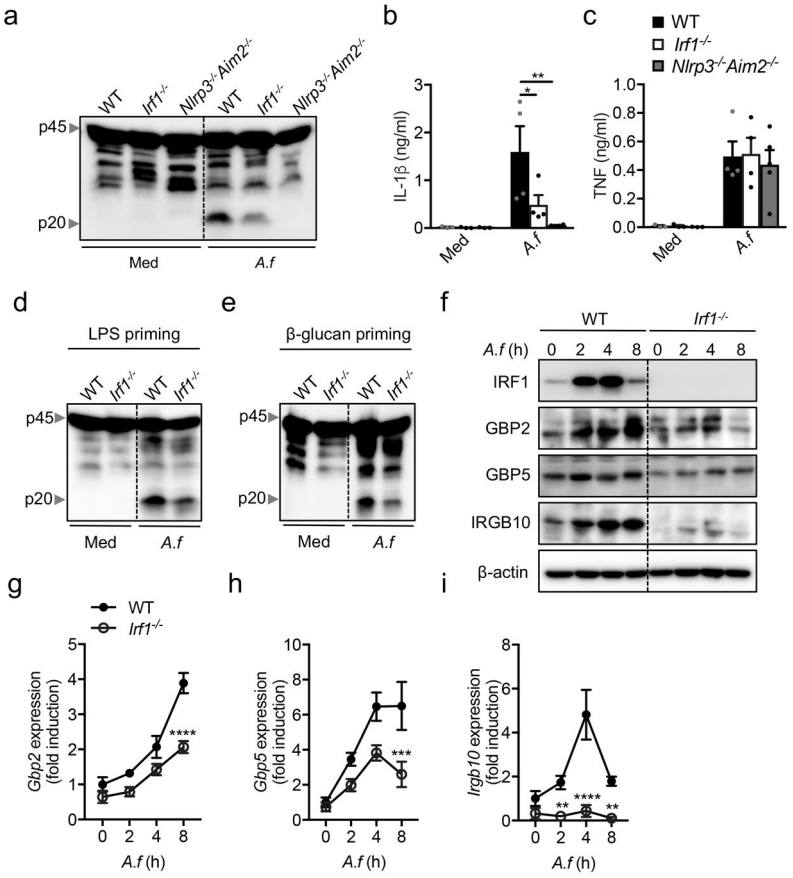

Figure 3. IRF1 regulates the expression of GBPs and IRGB10 upon *A. fumigatus* infection.

(**a**) Immunoblot analysis of caspase-1 (as in Fig. 1a), (**b**) release of IL-1β, and (**c**) TNF in unprimed WT and *Irf1*$^{-/-}$ BMDMs left uninfected (Med) or assessed after 20 h with *A.f* (MOI, 20), $n = 4$ biologically independent samples. (**d,e**) Immunoblot analysis of caspase-1 in LPS and β-glucan primed WT and *Irf1*$^{-/-}$ BMDMs assessed 20 h after infection with live *A.f* resting conidia (MOI, 20). (**f**) Immunoblot analysis of IRF1, GBP2, GBP5, and IRGB10 in unprimed WT and *Irf1*$^{-/-}$ BMDMs 0–8 h after infection with live *A.f* resting conidia (MOI, 20). (**g,h,i**) Real-time quantitative RT-PCR analysis of *Gbp2*, *Gbp5* and *Irgb10* genes in WT and *Irf1*$^{-/-}$ BMDMs 0–8 h after infection with *A.f* resting conidia (MOI, 20) presented relative to that of the gene encoding β-actin. *$P < 0.05$, **$P < 0.01$, ***$P < 0.001$, and ****$P < 0.0001$ (one-way ANOVA with Dunnett's multiple-comparisons test and Sidak's multiple-comparisons test), (**a–l**) Data are representative of at least 2 independent experiments (mean ± s.e.m.). The exact *P*-values are represented in the Supplementary Table 3.

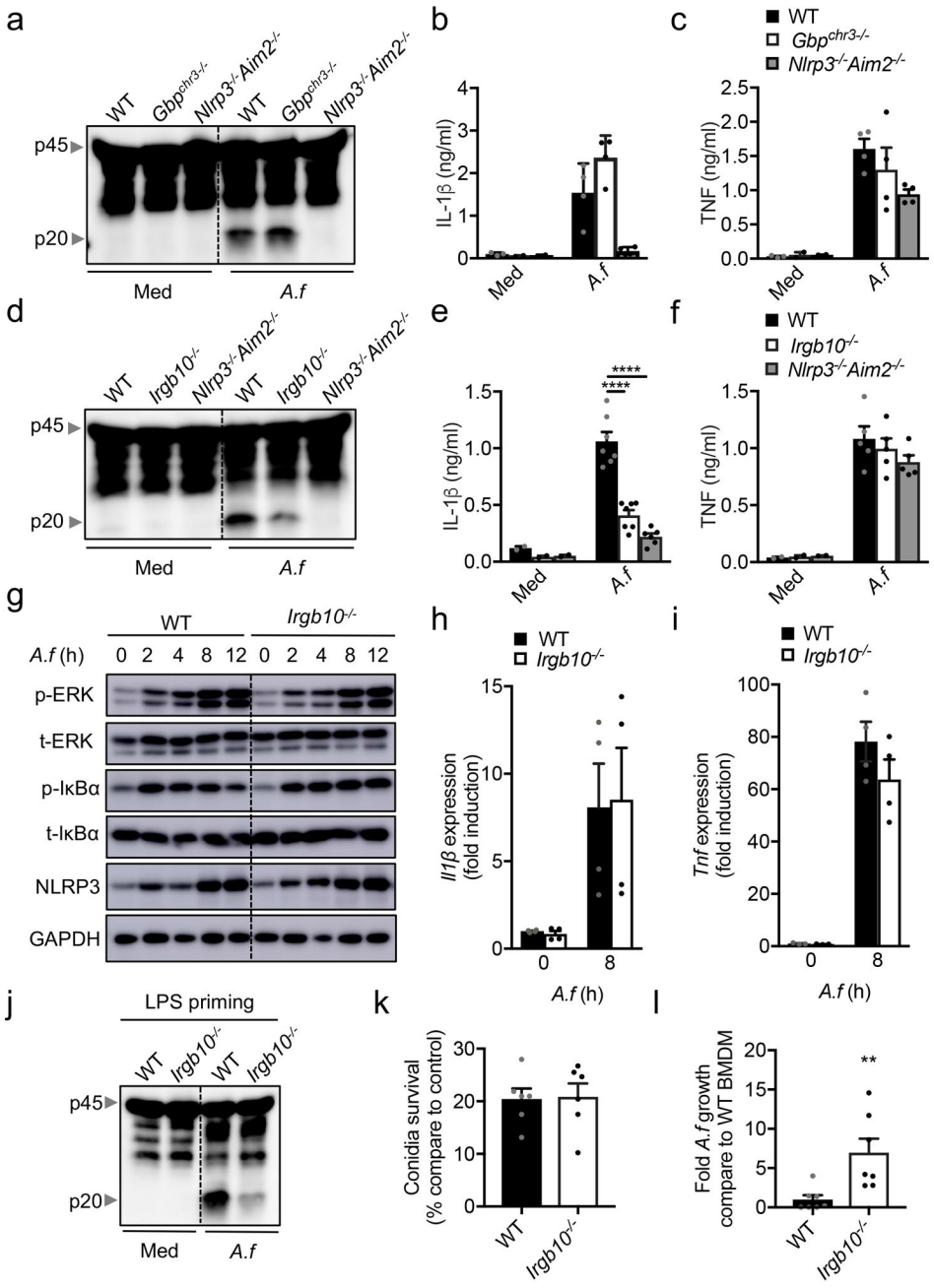

Figure 4. IRGB10 and not GBPs contributes to the activation of inflammasomes in response to *A. fumigatus*.

(**a,d**) Immunoblot analysis of caspase-1 (as in Fig. 1a), (**b,e**) release of IL-1β and (**c,f**) TNF by unprimed WT, (**a,b,c**) *Gbp*$^{chr3-/-}$ and (**d,e,f**) *Irgb10*$^{-/-}$ BMDMs left uninfected (Med) or assessed 20 h with *A.f* resting conidia (MOI, 20). (**b,c**) $n = 4$ biologically independent samples and (**e,f**) $n = 7$ biologically independent samples) (**g**) Immunoblot analysis of p-, t-ERK , p-, t-IκBα, and NLRP3 (as in Fig. 2d,e) in unprimed WT and *Irgb10*$^{-/-}$ BMDMs 0–12 h after infection with *A.f* resting conidia (MOI, 20). (**h,i**) Real-time quantitative RT-PCR analysis of *Il1β* and *Tnf* genes in WT and *Irgb10*$^{-/-}$ BMDMs 0–8 h after infection with *A.f* resting conidia (MOI, 20), presented relative to that of the gene encoding β-actin. (**j**)

Immunoblot analysis of caspase-1 in LPS primed WT and *Irgb10*$^{-/-}$ BMDMs assessed 20 h after infection with live *A.f* resting conidia (MOI, 20). (**k**) Conidiocidal activity of WT and *Irgb10*$^{-/-}$ BMDMs. (**l**) *A.f* hyphae inhibition assay of WT and *Irgb10*−/− BMDMs. **P* < 0.05, ***P* < 0.01, ****P* < 0.001, and *****P* < 0.0001 (one-way ANOVA with Dunnett's multiple-comparisons test and Sidak's multiple-comparisons test and unpaired t-test two tailed *P*-value). (**a–i**) Data are representative of at least 3 independent experiments (mean ± s.e.m.). The exact *P*-values are represented in the Supplementary Table 3.

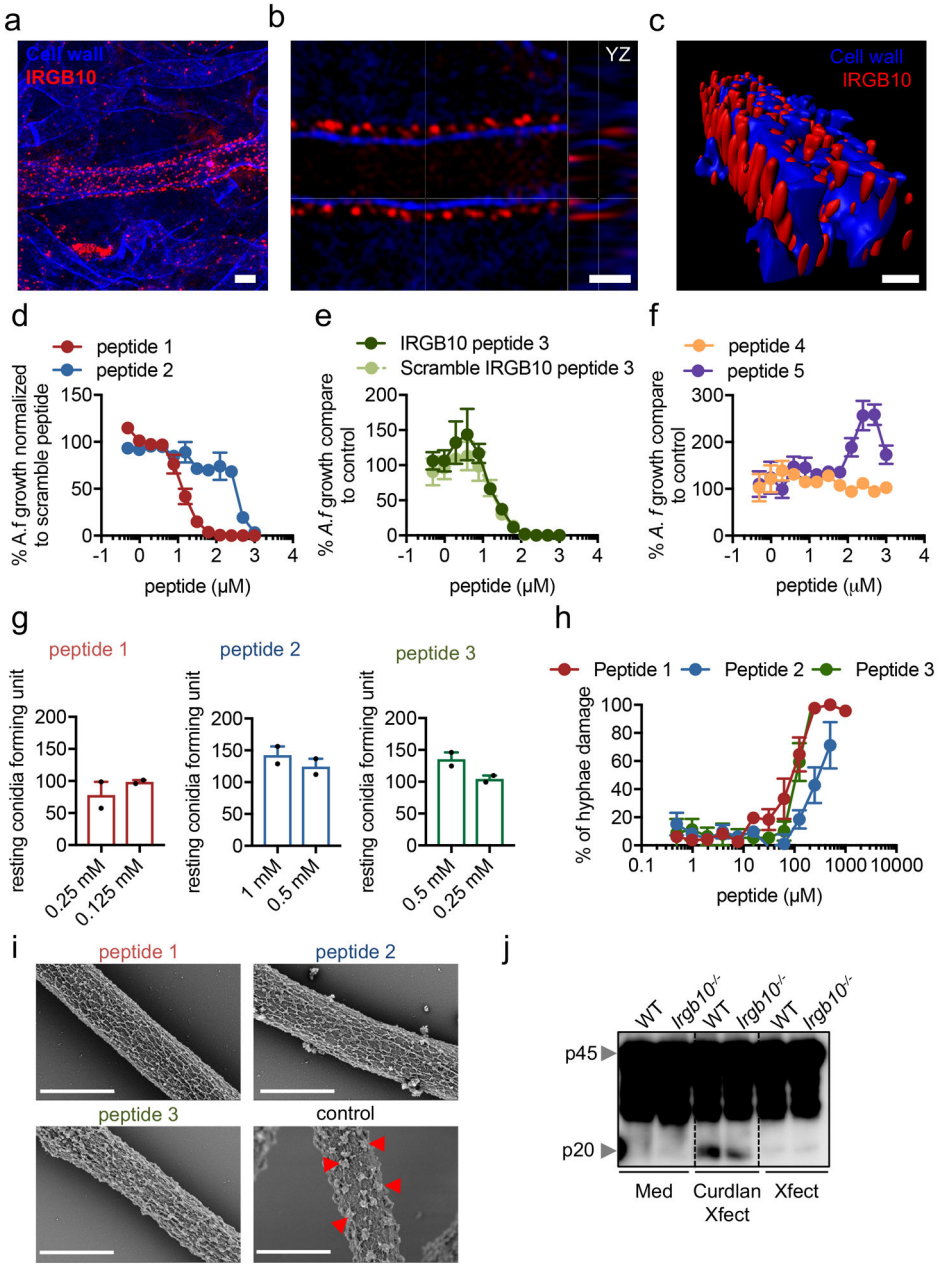

Figure 5. IRGB10 targets intracellular *A. fumigatus* and IRGB10 peptides inhibit *A. fumigatus* growth and release fungal ligands which induce inflammasome activation.

(**a–c**) Immunofluorescence staining of IRGB10 (red) and *A.f* cell wall (blue) in unprimed primary lung fibroblasts 16 h after infection with *A.f.* Images were taken by structured illumination microscopy (SIM), (**a**) A z-plane of a SIM image, (**b**) Orthogonal-image projection of *A.f.* (**c**) Three-dimensional projection of *A.f* hyphae presented in **b.** Scale bars 1 μm (**a–c**). (**d**) *A.f* growth in presence of increasing concentrations of IRGB10 peptides 1 and 2 respectively normalized to scramble petides 1 ($n = 4$ biologically independent samples) and 2 ($n = 5$ biologically independent samples), (**e**) *A.f* growth in increasing concentrations of IRGB10 peptides 3 and scramble peptide 3 ($n = 4$ biologically independent

samples), (**f**) peptide 4 and 5 normalized to vehicle control ($n = 6$ biologically independent samples). (**g**) Conidiocidal ($n = 2$ biologically independent samples) and (**h**) hyphae damage activity of IRGB10 peptides 1, 2 and 3 ($n = 5$ biologically independent samples), (**i**) Scanning electron microscopy surface analysis of *A.f* hyphae incubated for 5 h with IRGB10 peptides 1, 2, 3 and vehicle control, (**j**) Immunoblot analysis of pro-caspase-1 (p45) and the caspase-1 subunit p20 (p20) of unprimed BMDMs left untreated (medium alone [Med]) or assessed after curdlan transfection with Xfect (middle, [Curdlan Xfect]) or Xfect alone (right, [Xfect]). (**a-j**) Data are representative of at least 2 independent experiments (mean ± s.e.m.).

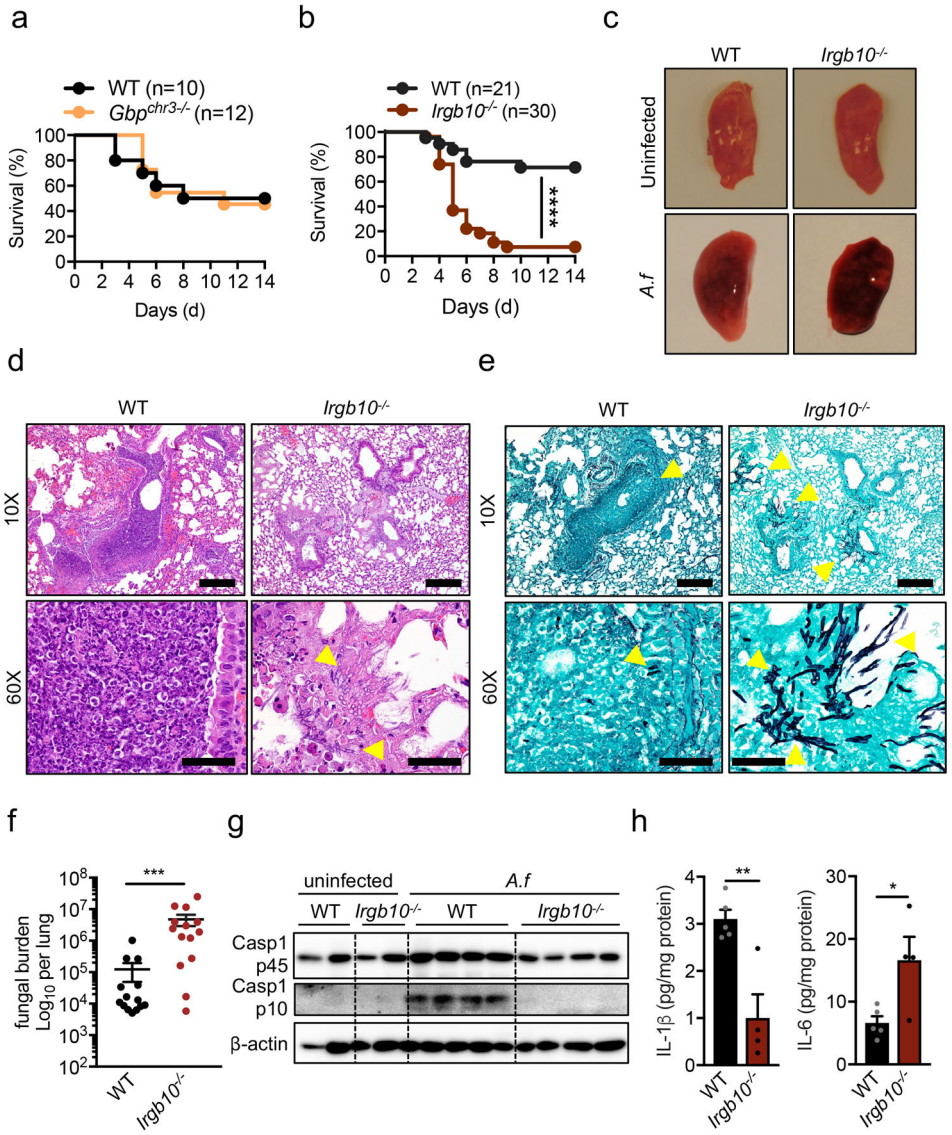

Figure 6. IRGB10 provides host protection against infection with *A. fumigatus in vivo*.

(**a**) Survival of 7- to 8-week-old wild-type mice ($n = 10$) and $Gbp^{chr3-/-}$ mice ($n = 12$) immunosuppressed with cyclophosphamide and cortisone acetate and infected intranasally with 5.5×10^5 of *A.f* resting conidia. (**b**) Survival of 7- to 8-week-old wild-type mice ($n = 21$) and $Irgb10^{-/-}$ mice ($n = 30$) infected intranasally with 5.5×10^5 of *A.f* resting conidia after immunosuppression with cyclophosphamide and cortisone acetate. (**c**) Macroscopic pathology of *A.f*–infected left lobe of lungs collected on day 4 post-infection or uninfected, pictures collected with camera, (**d**) Hematoxylin-and-eosin and (**e**) gomori methenamine silver staining and staining on day 4 after infection with *A.f.* (**f**) Real-time quantitative PCR analysis of *A.f* 18S rRNA levels in the lungs of WT and $Irgb10^{-/-}$ mice on day 4 after infection, WT and $Irgb10^{-/-}$ mice $n = 14$. (**g**) Immunoblot analysis of pro-caspase-1 (Casp-1, p45) and the caspase-1 subunit p10 (Caspl, p10) of lung homogenates after 4 days of infection with *A.f* resting conidia. (**h**) Levels of IL-1β and IL6 in lung homogenates after 2 days of infection with *A.f* resting conidia. $^{**}P < 0.01$ and $^{****}P < 0.0001$, (**a,b**) log-rank

(Mantel-Cox) test and (**f**) Mann-Whitney test two tailed P-value (**h**) unpaired t-test two tailed P-value. (**a,b**) Data are from 2 independents experiments and (**c–h**) data are representative of at least 1 experiment (mean ± s.e.m.). (**d,e**) Scale bars 200 μm (10X) and 50 pm (60X). The exact *P*-values are represented in the Supplementary Table 3.